THE AERODYNAMIC LOADING OF A STRUCTURALLY DEFORMED DELTA WING AT SUPERSONIC SPEEDS

By

John L. Troutman

Thesis submitted to the Graduate Faculty of the
Virginia Polytechnic Institute

in candidacy for the degree of

MASTER OF SCIENCE

in

Applied Mechanics

August 1956

THE AERODYNAMIC LOADING OF A STRUCTURALLY DEFORMED DELTA WING AT SUPERSONIC SPEEDS

by

John L. Troutman

Thesis submitted to the Graduate Faculty of the

Virginia Polytechnic Institute

in candidacy for the degree of

MASTER OF SCIENCE

in

Applied Mechanics

APPROVED:

Director of Graduate Studies

APPROVED:

Head of Department

Dean of Engineering

Supervisor

August 1956

Blacksburg, Virginia

TABLE OF CONTENTS

I. LIST OF FIGURES

II. LIST OF SYMBOLS

$2a$	nondimensional body width
c_R	root chord dimension
l	exposed semispan dimension
K_1, K_2	quantities defined in equations (22) and (31)
L.E., T.E.	abbreviations for leading edge and trailing edge, respectively
m	modified aspect-ratio parameter defined by $m = \frac{8l}{c_R}$
M	free-stream Mach number
p	lift per unit area
q	dynamic pressure defined by $q = \frac{1}{2}\rho V^2$
R_1, R_2, R_3	quantities defined in equations (21), (29), and (30)
S_D, S_E, S_W	areas of integration identified in Appendix A
V	free-stream velocity
$l(y_1)$	distributed spanwise lift measured positive upward
$m(y_1)$	distributed spanwise moment about trailing edge taken as positive leading edge up
$\eta(y_1)$	distributed spanwise second moment about trailing edge
α	constant angle of attack
β	Mach number parameter defined by $\beta = \sqrt{M^2 - 1}$
$\gamma(y_1)$	chordwise curvature distribution
$\theta(y_1)$	trailing-edge angle-of-attack distribution
$\sigma(x_1, y_1)$	general angle-of-attack distribution
$\varphi(x_1, y_1)$	perturbation velocity potential
ρ	free-stream density

Coordinate systems:

x,y or η,z	conventional dimensional coordinates in chordwise, spanwise, and vertical directions, respectively
x_1,ξ_1	nondimensional chordwise coordinates defined by $x_1 = \frac{x}{c_R}$
y_1 or η_1	nondimensional spanwise coordinates defined by $y_1 = \frac{y}{l}$, $\eta_1 = \frac{\eta}{l}$

Subscripts:

A	denotes antisymmetrical deformation
S	denotes symmetrical deformation
γ	refers to angle-of-attack distribution of $\gamma(y_1)$
θ	refers to angle-of-attack distribution of $\theta(y_1)$
σ	refers to general angle-of-attack distribution

III. INTRODUCTION

The advent of high-speed flight of low-aspect-ratio lifting surfaces has brought with it the recognition of the importance of the aeroelastic behavior of such structures. By aeroelastic behavior is meant the response of the flexible, elastic surface to its aerodynamic loading in flight. The structurally deformed wing thus experiences additional aerodynamic loading to that which would be present if the wing were rigid. This additional loading may serve as a damping factor by decreasing the effective angle of attack, and hence the loading; or it may tend to increase the angle of attack resulting in increased loading to the point of failure, as in wing torsional divergence. Thus it is seen that knowledge of the aerodynamic "structural" loading of wing surfaces is important to the successful design of high-speed aircraft.

In the present state of theoretical development (reference 5), the complexity of aeroelastic analyses necessitates the use of linearized theories - both structural and aerodynamic. In linearized aerodynamic theory, it is possible to separate that part of the angle-of-attack distribution of a surface furnished by its structural deformation from the whole, and consider its effects independently. Since the behavior of the rigid surface is known, in general, it is only necessary to analyse the deformed surface and its resultant loading. Such an analysis was performed by Hedgepeth and Kell (reference 3) in connection with the aeroelastic rolling behavior of a rectangular wing at steady supersonic speeds.

An aeroelastic analysis of the type employed in the above reference divides itself naturally into three parts:

(1) The determination of the deformations of the surface (with reference to its angle-of-attack distribution) resulting from an arbitrary loading

(2) The determination of the aerodynamic loading of the surface resulting from an arbitrary angle-of-attack distribution

(3) The formulation of the aeroelastic problem by a proper combination of the above structural and aerodynamic ingredients, and the resulting solution, if possible.

The delta configuration is one of the more popular high-speed lifting surfaces at present. Furthermore, the present design trend of thicker cover sheets with minimum amounts of chordwise stiffening would result (in the limit) in thin, solid wings.

A structural analysis of thin, solid delta wings, suitable for incorporation in an aeroelastic analysis similar to that outlined above, has been performed and experimentally verified (reference 1). In this thesis, the aerodynamic loading of such a delta configuration resulting from its arbitrary structural deformation in steady flight is obtained.

The derivation was guided by the structural analysis (reference 1) to the extent of specifying the chordwise deflection shape, and covers both symmetrical and antisymmetrical angle-of-attack distributions. The results are presented in influence function form and can thus be applied to determine the loading of the delta wing resulting from other angle-of-attack distributions than that furnished by its structural deformation.

IV. ANALYSIS

It is desired to determine the aerodynamic loading imposed on a thin, flexible, delta wing resulting from its structural deformation in steady supersonic flight. Linearized aerodynamics will be assumed throughout the analysis.

The general configuration to be analyzed consists of a pair of thin, solid flexible wings of triangular plan form attached along root lines to a rigid rectangular plate corresponding to a fuselage section. The model is placed horizontally in an airstream of Mach number M parallel to the fuselage center line. In this position the leading edges are swept back and the trailing edges are unswept.

The origin of coordinates is chosen at the intersection of the trailing edge and the right root line (when viewed from the trailing edge forward). In accordance with standard aerodynamic convention, the x axis is taken in the streamwise direction, and the y axis runs outboard along the right wing trailing edge. The z (or w) axis is then taken as positive upward, thus furnishing a right hand system. A labeled sketch of the configuration is given in Figure 1 together with the coordinate system chosen.

For convenience, the coordinates in the plane of the wing are nondimensionalized with respect to reference dimensions of the surface; the x coordinate is nondimensionalized with respect to the root chord length c_R and the y coordinate with respect to the exposed wing semispan l. The process is completed by specifying the nondimensional body width as $2a$.

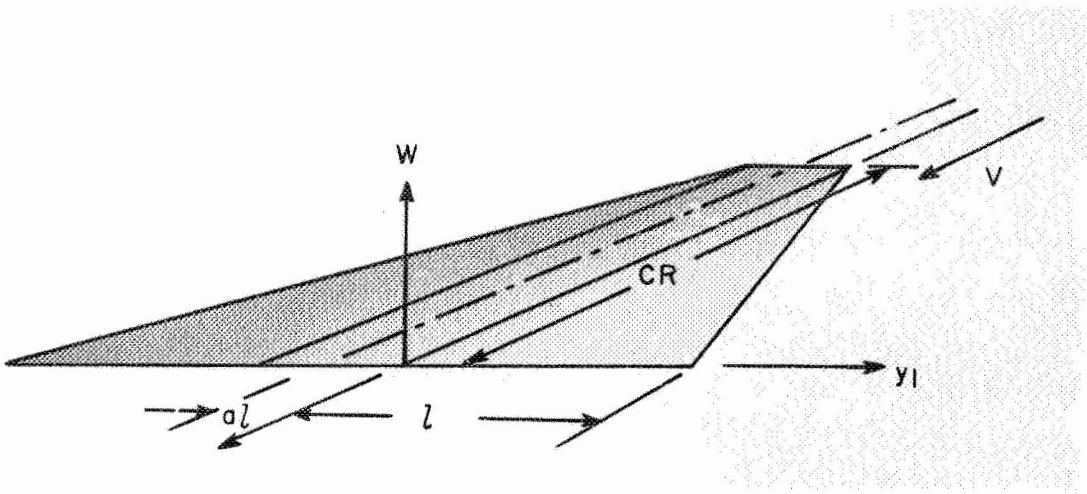

Figure 1.- General configuration considered with dimensional coordinates given.

The fuselage or body section is held at zero angle of attack everywhere, while the flexible wings are allowed to deform either symmetrically or antisymmetrically with respect to the fuselage center line. If the local angle of attack for the right wing is given in nondimensional coordinates by $\sigma(x_1, y_1)$, then symmetrical deformation (Figure 2(a)) is characterized by

$$\sigma(x_1, -2a - y_1) = \sigma(x_1, y_1) \tag{1}$$

and antisymmetrical deformation (Figure 2(b)) by

$$\sigma(x_1, -2a - y_1) = -\sigma(x_1, y_1) \tag{2}$$

From the symmetry (or antisymmetry) of the deformation, it is seen that the resulting aerodynamic loading must also be symmetrical (or antisymmetrical) in the same manner. Hence it will be sufficient to determine the loading for the right wing alone produced by the angle-of-attack distribution of both wings.

Structural analyses of thin solid triangular wings of the type considered here were made in reference 1. Influence coefficients were calculated by assuming both linear and parabolic deflections of the wing in the chordwise direction. Comparison with experimental results revealed that the parabolic term must be included in the assumed chordwise deflection shape in order to obtain good agreement with the measured angles of attack. The most general angle-of-attack distribution resulting from this assumption varies linearly chordwise and can be written for the right wing as:

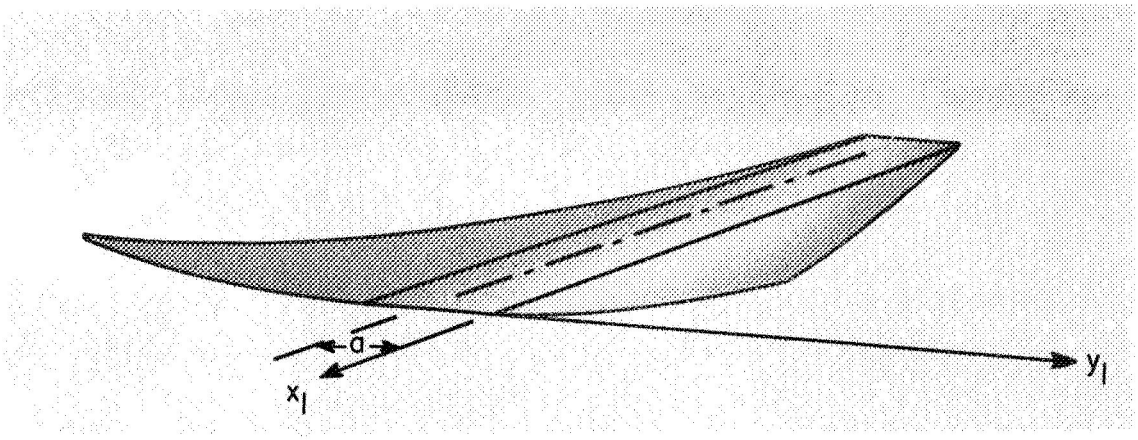

(a) Symmetrical deformation. $\sigma(x_1, -y_1 - 2a) = \sigma(x_1, y_1)$.

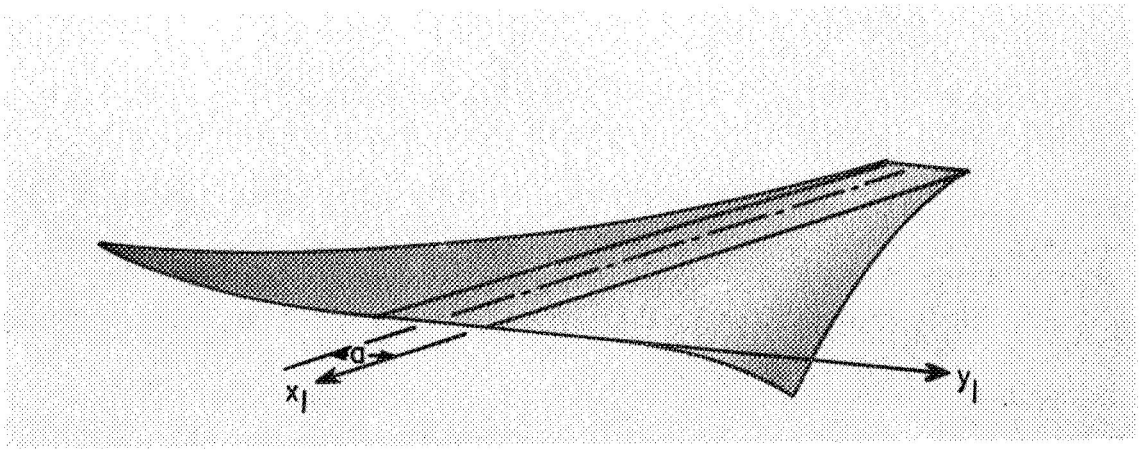

(b) Antisymmetrical deformation. $\sigma(x_1, -y_1 - 2a) = -\sigma(x_1, y_1)$.

Figure 2.- General deformations considered.

$$\alpha(x_1, y_1) = \theta(y_1) + x_1 c_R \gamma(y_1) \qquad (3)$$

where $\theta(y_1)$ and $\gamma(y_1)$ are arbitrary spanwise functions. $\theta(y_1)$ describes the angle-of-attack distribution at the trailing edge, and $\gamma(y_1)$ is proportional to the chordwise curvature distribution.

From the energy methods approach of reference 1, it is seen that in order to produce the required parabolic chordwise deflection shape, it is necessary to apply distributed spanwise lifts, moments, and second moments. Accordingly, it is desired to determine these aerodynamic loading functions for the deformed wing. Because of the linearized aerodynamics it is possible to separate the assumed angle-of-attack distribution (equation (3)) into two parts $\theta(y_1)$ and $x_1 c_R \gamma(y_1)$, and to determine the loading for each part independently. Therefore, the distributed spanwise lift taken as positive upward resulting from an angle-of-attack distribution of $\theta(y_1)$ is defined as $l_\theta(y_1)$ and that associated with the angle-of-attack distribution of $c_R x_1 \gamma(y_1)$ is defined as $l_\gamma(y_1)$. Similarly the distributed spanwise moments about the trailing edge taken positive leading edge up are defined respectively as $m_\theta(y_1)$ and $m_\gamma(y_1)$ and the distributed second moments about the trailing edge are defined as $n_\theta(y_1)$ and $n_\gamma(y_1)$.

In order to obtain the loading imposed by an arbitrary angle-of-attack distribution of the form of equation (3), resort is made to the step-super position techniques first used by Frick and Chubb (reference 2). For convenience and understanding of the method, the

derivation is given somewhat rigorously in the appendix of this Thesis. There, for any finite wing surface, such as the one considered here, it is shown by linear system theory that, if a positive unit step angle of attack given by $\alpha(x_1, y_1) = 1(y_1 - \eta_1)$ gives rise to the indicial lift distribution $l_\theta^*(y_1, \eta_1)$, then an arbitrary angle of attack of $\theta(y_1)$ would produce the section lift:

$$l_\theta^*(y_1) = \int_0^1 l_\theta^*(y_1, \eta_1) \frac{\partial \theta(\eta_1)}{\partial \eta_1} d\eta_1 \qquad (4)$$

Here $1(y_1 - \eta_1)$ is the well-known step function defined by

$$1(y_1 - \eta_1) = \begin{cases} 0, & y_1 < \eta_1 \\ 1, & y_1 > \eta_1 \end{cases}$$

And it follows that if a unit curvature step angle of attack of $\alpha(x_1, y_1) = x_1 1(y_1 - \eta_1)$ gives rise to the indicial lift distribution $l_\gamma^*(y_1, \eta_1)$, then an arbitrary angle of attack of $x_1 c_R \gamma(y_1)$ would produce the section lift

$$l_\gamma^*(y_1) = \int_0^1 l_\gamma^*(y_1, \eta_1) \frac{\partial c_R \gamma(\eta_1)}{\partial \eta_1} d\eta_1 \qquad (5)$$

and similarly for the moment and second moment loading functions. The hypothetical unit step angle-of-attack distributions $1(y_1 - \eta_1)$ and $x_1 1(y_1 - \eta_1)$ may be thought of as corresponding to a deflected flap over a portion of a wing surface. It is assumed that the gap is sealed

between the deflected and undeflected regions of the surface by a vertical membrane. Both of these distributions are shown in Figure 3. It is seen that the second gives, effectively, a negative angle-of-attack distribution over the deflected region.

The aerodynamic character of a supersonic delta wing is found to depend on the modified aspect-ratio parameter m, defined by $m = \frac{\beta l}{c_R}$ where $\beta = \sqrt{M^2 - 1}$ for a Mach number M; and $\frac{l}{c_R}$ is the aspect ratio of the exposed wing. The significance of this parameter will be discussed later in the thesis. There, it will be shown that for $m > \frac{1}{1 + 2a}$ where $2a$ is the nondimensional body width, the above equations may be applied to each wing independently, and the results appropriately combined to obtain the desired loading for the entire delta configuration.

This restriction $\left(\text{that is, } m > \frac{1}{1 + 2a}\right)$ will be assumed throughout the remainder of the analysis so that the above separation of effects is possible. The result is that the dependence of the loading on the body width is removed. Thus, for the symmetrically deformed wing, it is apparent that the lift on either wing resulting from the angle-of-attack distribution of the other is identical at corresponding spanwise stations. Therefore, the partial section lift on the right wing resulting from a symmetrical angle of attack of $\theta(y_1)$ is given by (see equation (1))

$$l_\theta(y_1)\Big]_s = l_\theta^*(y_1) + l_\theta^*(-y_1 - 2a) \tag{6}$$

while analogous reasoning gives for the partial section lift on the right wing resulting from an antisymmetrical angle of attack of $\theta(y_1)$ (see equation (2))

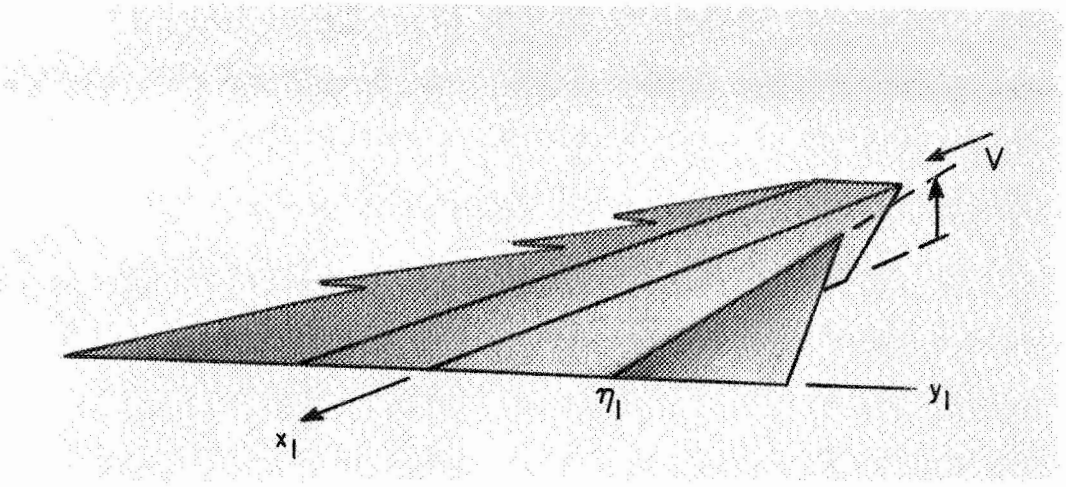

(a) $\sigma(x_1, y_1) = 1(y_1 - \eta_1)$.

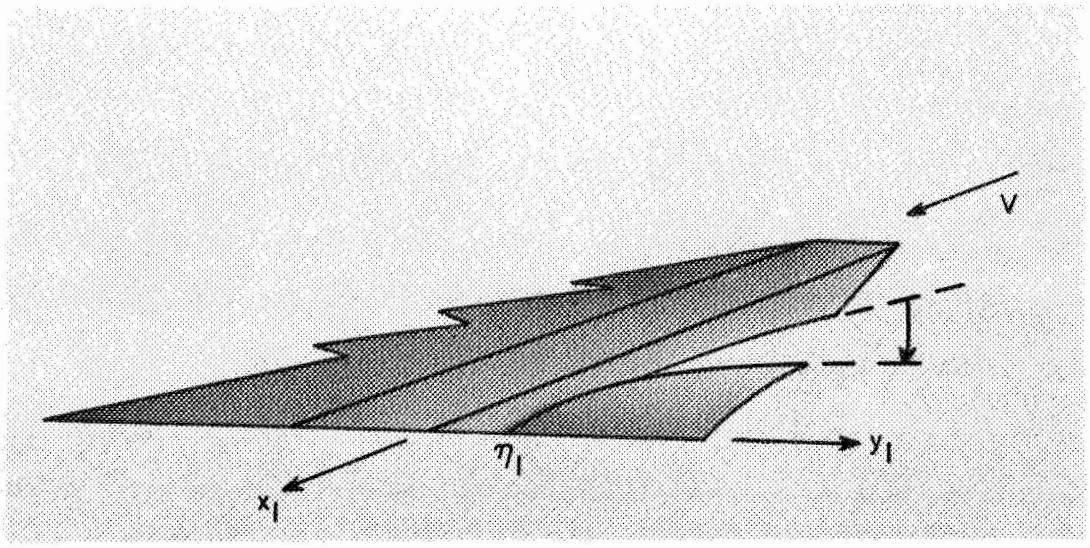

(b) $\sigma(x_1, y_1) = x_1 1(y_1 - \eta_1)$.

Figure 3.- Illustrations of indicial angle-of-attack distributions.

$$l_\theta(y_1)\Big]_A = l_\theta^*(y_1) - l_\theta^*(-y_1 - 2a) \tag{7}$$

and similarly for the section lift resulting from an angle-of-attack distribution of $x_1 c_R \gamma(y_1)$. The subscripts S and A refer to symmetrical and antisymmetrical deformations, respectively.

Finally, the total section lift on the right wing resulting from the assumed angle-of-attack distribution (equation (3)) is obtained for the symmetrically (or antisymmetrically) deformed wing by superposing the partial section lifts (see equations (6) and (7)).

Thus:

$$l(y_1)\Big]_S = l_\theta(y_1)\Big]_S + l_\gamma(y_1)\Big]_S \tag{8}$$

$$l(y_1)\Big]_A = l_\theta(y_1)\Big]_A + l_\gamma(y_1)\Big]_A \tag{9}$$

The above determination of total section lift was selected as an example. The analysis and resulting equations can be applied in a similar manner to determine the total section moments on the right wing. It now remains only to derive the aerodynamic indicial loading functions.

From linearized steady flow theory the lift per unit area of a thin wing at an angle of attack $\sigma(x_1, y_1)$ is given by

$$p_\sigma(x_1, y_1) = \frac{4q}{Vc_R} \frac{\partial \sigma_\sigma(x_1, y_1)}{\partial x_1} \tag{10}$$

where V is the velocity of the free stream; q is the dynamic pressure defined by $q = \frac{1}{2}\rho V^2$ for a flow density ρ; c_R is the

root chord dimension; and $\varphi_\sigma(x_1, y_1)$ is the well-known perturbation velocity potential resulting from the given angle-of-attack distribution.

The resulting section loading is determined by integrating the pressure distribution across the local chord. Thus

$$l_\sigma(y_1) = c_R \int_{L.E.}^{T.E.} p_\sigma(x_1, y_1)dx_1 = \frac{\rho q}{V c_R} \varphi_\sigma(0, y_1) \tag{11}$$

$$m_\sigma(y_1) = -c_R^2 \int_{L.E.}^{T.E.} x_1 p_\sigma(x_1, y_1)dx_1 = \frac{\rho q}{V c_R} \int_{L.E.}^{T.E.} \varphi_\sigma(x_1, y_1)dx_1 \tag{12}$$

$$-n_\sigma(y_1) = c_R^3 \int_{L.E.}^{T.E.} x_1^2 p_\sigma(x_1, y_1)dx_1$$

$$= -\frac{8q}{V c_R} \int_{L.E.}^{T.E.} x_1 \varphi_\sigma(x_1, y_1)dx_1 \tag{13}$$

where L.E. and T.E. refer to leading edge and trailing edge, respectively. The final forms of equations (11)-(13) are obtained by substituting equation (10), integrating by parts, and utilizing the fact that the potential must vanish at the leading edge.

The problem is now reduced to the determination of the indicial potential functions $\varphi_\theta(x_1, y_1)$ and $\varphi_\gamma(x_1, y_1)$ associated respectively with step angles of attack of $1(y_1 - \eta_1)$ and $x_1 1(y_1 - \eta_1)$. From these the indicial loading functions can be determined by equations (11)-(13) and from the indicial loading functions, the total section loading is given through equations (4)-(9). A similar problem arose in connection with an aeroelastic analysis of a supersonic rectangular wing (reference 3)

and was attacked successfully by utilising the linearised lifting surface theory of Evvard (reference 4). The elements of this theory are presented in the Appendix for convenience and discussed. Briefly, however, the method involves the well-known technique of replacing the wing surface by a sheet of supersonic sources with strengths proportional to the local slope. The potential at a point (x_1, y_1) on the wing surface is then determined by integrating the source potential distribution over a portion of the surface contained within the Mach forecone of the point.

Thus, for an angle-of-attack distribution of $\sigma(x_1, y_1)$

$$\varphi_\sigma(x_1, y_1) = \frac{V_1}{\pi} \iint_{S_E} \frac{\sigma(\xi_1, \eta_1)\, d\xi_1\, d\eta_1}{\sqrt{(x_1 - \xi_1)^2 - m^2(y_1 - \eta_1)^2}} \qquad (14)$$

S_E, the Evvard area of integration, is defined and discussed in the Appendix. The general characteristics of the area are found to depend on the aforementioned modified aspect-ratio parameter, m. For $m > 1$, the leading edge of the wing is supersonic. That is, the component of flow velocity normal to the leading edge is supersonic and the leading edges are coincident with the Mach wave, the envelope of the foremost Mach aftercones of the wing. For $m < 1$, however, the leading edges are subsonic and lie behind or within the foremost Mach wave giving rise to a disturbed flow field region which influences the pressures on the wing surface. It is therefore necessary to consider these cases separately. At an earlier point a lower value of m was given $\left(m > \frac{1}{1 + 2a}\right)$. This restriction establishes the boundary for which

points on the wing surface are influenced by at most a single external flow field. At the critical value, the Mach cone from the apex of either wing passes through the tip of the opposite wing. Below this value of $m_{,}$ it would be necessary to consider the entire delta surface as a unit. The methods of Evvard can readily be extended to cover these cases (see reference 4); however, it is felt that the reduced range of applicability would not justify the required additional effort. By restricting m to values above $\frac{1}{1+2a'}$, it is possible to consider the right wing as extending along its leading and trailing edges to infinity at the left. It is then only necessary to calculate the potentials and resulting loading for this model alone. Finally, from equation (14) and the assumed step angle-of-attack distributions, it is evident that the effective S_g will be terminated at the step station η_1, that is, S_g will not extend inboard of this station.

The results of this analysis and discussion follow.

Case I: Subsonic Leading Edges ($m < 1$)

For subsonic leading edges, a step angle-of-attack distribution of the types described divides the semi-infinite wing model into three regions through the action of the reflected Mach wave (see Appendix). These regions and the effective S_g for the potential at a point in each are shown in Figure 4(a).

The required integrations (equations (11)-(14)) necessary to derive the aerodynamic indicial loading functions are straightforward though tedious and only the results will be presented here. It should

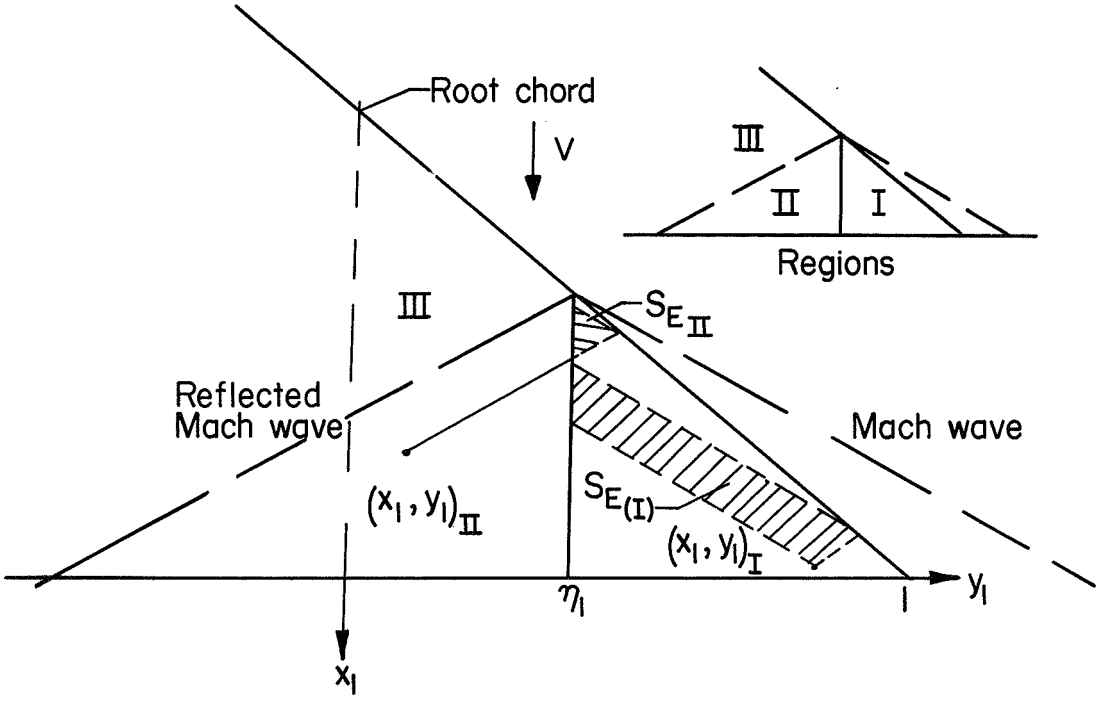

(a) Subsonic leading edge ($m < 1$).

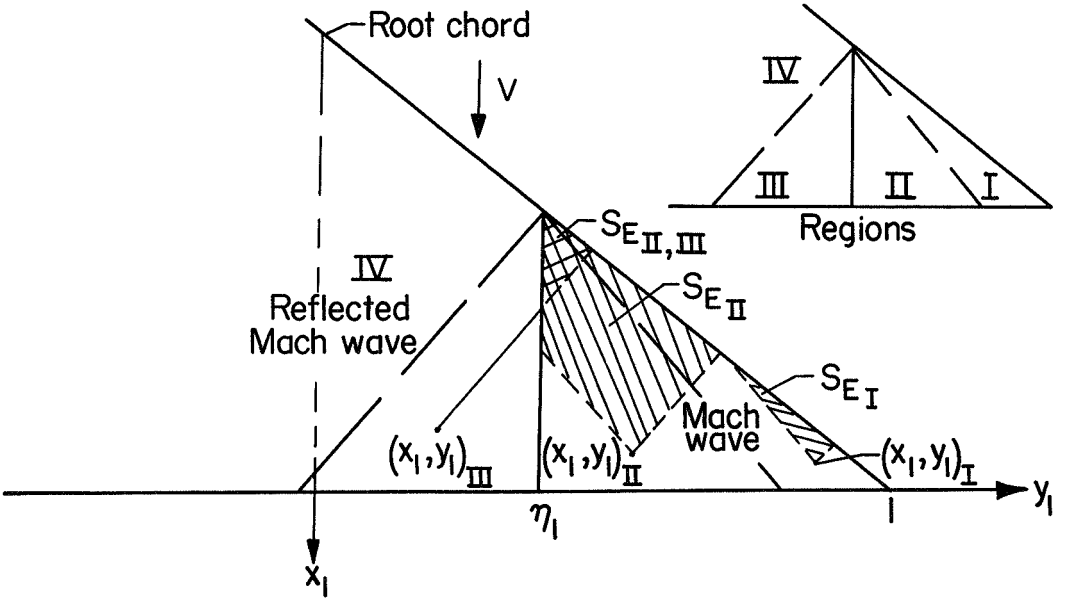

(b) Supersonic leading edge ($m > 1$).

Figure 4.- S_E for determination of indicial potential functions.

be remarked, however, that the integrations required to determine the potential are greatly facilitated by the introduction of the Mach wave or characteristic coordinates of Evvard.

For $\eta_1 - \frac{1 - \eta_1}{m} \leq y_1 \leq 1$

$$i_\theta^*(y_1, \eta_1) = q \frac{c_R}{\beta}\left(\frac{8m}{\pi(m+1)}\left[R_1 + (y_1 - \eta_1)(m+1)\tanh^{-1}K_1\right]\right) \tag{15}$$

$$m_\theta^*(y_1, \eta_1) = q \frac{c_R^2}{\beta}\left(\frac{2m}{\pi(m+1)}\left\{\left[2 - y_1(m+3) + \eta_1(m+1)\right]R_1 + (y_1 - \eta_1)(m+1)\left[4 + y_1(m-3) - \eta_1(m+1)\right]\tanh^{-1}K_1\right\}\right) \tag{16}$$

$$n_\theta^*(y_1, \eta_1) = q \frac{c_R^3}{\beta}\left(\frac{8m}{\pi(m+1)}\left\{\left[\frac{(1-\eta_1)^2}{3} - \frac{(1-\eta_1)(y_1-\eta_1)(5m+13)}{12} - \frac{(3m+5)(m-3)(y_1-\eta_1)^2}{24}\right]R_1 + \left[(1-\eta_1)^2 + \frac{(y_1-\eta_1)(1-\eta_1)(m-3)}{2} + \frac{(y_1-\eta_1)^2(m^2-2m+5)}{8}\right](y_1-\eta_1)(m+1)\tanh^{-1}K_1\right\}\right) \tag{17}$$

$$i_y^*(y_1, \eta_1) = q \frac{c_R}{\beta}\left(-\frac{16m^2}{3\pi(m+1)^2}\left[1 - \eta_1 + m(y_1 - \eta_1)\right]R_1\right) \tag{18}$$

$$n_y^*(y_1, \eta_1) = q\frac{\sigma_R^2}{\beta}\left(-\frac{16m^2}{3\pi(m+1)^2}\left\{\frac{R_1^3}{3}+\right.\right.$$

$$\frac{(m+1)(y_1-\eta_1)}{8}\left[\left[2(1-\eta_1)+(m-1)(y_1-\eta_1)\right]R_1-\right.$$

$$\left.\left.(m+1)^2(y_1-\eta_1)^2\tanh^{-1}K_1\right]\right\}-\left.\frac{\beta n_\theta^*(y_1,\eta_1)}{2q\sigma_R^3}\right) \qquad (19)$$

$$n_y^*(y_1, \eta_1) = q\frac{\sigma_R^3}{\beta}\left(-\frac{32m^2}{3\pi(m+1)^2}\left\{\left[\frac{1-\eta_1}{12}-\left(\frac{5}{3}+m\right)\frac{(y_1-\eta_1)}{8}\right]R_1^3+\left[1-\eta_1+\right.\right.\right.$$

$$\frac{(3m-5)(y_1-\eta_1)}{8}\left]\left[\frac{2(1-\eta_1)+(m-1)(y_1-\eta_1)}{8}\right](m+1)(y_1-\eta_1)R_1-\right.$$

$$\left.\left[\frac{(3m-5)(y_1-\eta_1)}{64}+\frac{1-\eta_1}{8}\right](m+1)^3(y_1-\eta_1)^3\tanh^{-1}K_1\right\}-$$

$$\frac{16m}{3\pi(m+1)}\left\{\left[\frac{(1-\eta_1)^3}{4}-\frac{(y_1-\eta_1)(1-\eta_1)^2(13m+31)}{24}-\right.\right.$$

$$\frac{(y_1-\eta_1)^2(1-\eta_1)(31m^2-42m-145)}{96}-$$

$$\left.\frac{(y_1-\eta_1)^3(15m^3-17m^2+25m+105)}{192}\right]R_1+\left[(1-\eta_1)^3+\right.$$

$$\tfrac{3}{4}(y_1-\eta_1)(1-\eta_1)^2(m-3)+\tfrac{3}{8}(y_1-\eta_1)^2(1-\eta_1)(m^2-2m+5)+$$

$$\left.\left.\left.\frac{(y_1-\eta_1)^3(5m^3-9m^2+15m-35)}{64}\right](m+1)(y_1-\eta_1)\tanh^{-1}K_1\right\}\right) \qquad (20)$$

where

$$R_1 \equiv \sqrt{\left[1 + my_1 - \eta_1(1 + m)\right]\left[1 - y_1\right]} \tag{21}$$

$$K_1 \equiv \begin{cases} \sqrt{\dfrac{1 + my_1 - \eta_1(1 + m)}{1 - y_1}}, & \eta_1 - \dfrac{1 - \eta_1}{m} \le y_1 \le \eta_1 \\ \sqrt{\dfrac{1 - y_1}{1 + my_1 - \eta_1(1 + m)}}, & \eta_1 \le y_1 \le 1 \end{cases} \tag{22}$$

Case II: Supersonic Leading Edges ($m > 1$)

For supersonic leading edges, the step angle of attack with the action of the Mach waves divides the wing surface into four regions. For this case the reflection techniques of Evvard are unnecessary and the potential at a point is determined by integrating over the entire wing surface contained within the Mach forecone of the point. These regions and the effective S_E for a point in each are shown in Figure 4(b).

Again the required integrations are tedious and only the results will be given here.

For $\eta_1 - \dfrac{1 - \eta_1}{m} \le y_1 \le 1$:

$$\left.\begin{aligned} l_\theta^*(y_1, \eta_1) &= q\,\frac{c_R}{\beta}\left(\frac{\delta m}{\pi}\left[\frac{(1 - y_1)}{\sqrt{m^2 - 1}}\tan^{-1}R_2 + (y_1 - \eta_1)\tanh^{-1}K_2\right]\right), \\ &\qquad \eta_1 - \frac{1 - \eta_1}{m} \le y_1 < \eta_1 + \frac{1 - \eta_1}{m} \\ l_\theta^*(y_1, \eta_1) &= q\,\frac{c_R}{\beta}\left(\frac{\delta m(1 - y_1)}{\sqrt{m^2 - 1}}\right), \\ &\qquad \eta_1 + \frac{1 - \eta_1}{m} \le y_1 \le 1 \end{aligned}\right\} \tag{23}$$

$$
\left.
\begin{aligned}
m_\Theta^*(y_1, \eta_1) &= q\,\frac{c_R^2}{\beta}\left(\frac{1}{\pi}\left[\frac{(1-y_1)^2}{\sqrt{m^2-1}}\tan^{-1}R_3 - \frac{(y_1-\eta_1)}{2}R_3 + (y_1-\eta_1)(2-\eta_1-y_1)\tanh^{-1}K_2\right]\right), \\
&\qquad \eta_1 - \frac{1-\eta_1}{m} \le y_1 < \eta_1 + \frac{1-\eta_1}{m} \\
m_\Theta^*(y_1, \eta_1) &= q\,\frac{c_R^2}{\beta}\left(\frac{2m(1-y_1)^2}{\sqrt{m^2-1}}\right), \\
&\qquad \eta_1 + \frac{1-\eta_1}{m} \le y_1 \le 1
\end{aligned}
\right\} \quad (24)
$$

$$
\left.
\begin{aligned}
n_\Theta^*(y_1, \eta_1) &= q\,\frac{c_R^3}{\beta}\left(\frac{8m}{3\pi}\left\{\frac{(1-y_1)^3}{\sqrt{m^2-1}}\tan^{-1}R_2 + \frac{(y_1-\eta_1)\left[2(y_1-\eta_1)-5(1-\eta_1)\right]}{4}R_3 + \left[3(1-\eta_1)(1-y_1) + \frac{(y_1-\eta_1)^2(m^2+2)}{2}\right](y_1-\eta_1)\tanh^{-1}K_2\right\}\right) \\
&\qquad \eta_1 - \frac{1-\eta_1}{m} \le y_1 < \eta_1 + \frac{1-\eta_1}{m} \\
n_\Theta^*(y_1, \eta_1) &= q\,\frac{c_R^3}{\beta}\left(\frac{1}{3}\frac{(1-y_1)^3}{\sqrt{m^2-1}}\right), \\
&\qquad \eta_1 + \frac{1-\eta_1}{m} \le y_1 \le 1
\end{aligned}
\right\} \quad (25)
$$

$$
\left.
\begin{aligned}
i_y^*(y_1, \eta_1) &= q\frac{c_R}{\beta}\left(-\frac{\lambda m}{\pi}\left\{\frac{m^2(1-y_1)^2}{(m^2-1)^{3/2}}\tan^{-1}R_2 - \frac{\left[1-\eta_1-m^2(y_1-\eta_1)\right]}{2(m^2-1)}R_3\right\}\right), \\
&\qquad \eta_1 - \frac{1-\eta_1}{m} \le y_1 < \eta_1 + \frac{1-\eta_1}{m} \\
i_y^*(y_1, \eta_1) &= q\frac{c_R}{\beta}\left(-\frac{2m^3}{(m^2-1)^{3/2}}(1-y_1)^2\right), \\
&\qquad \eta_1 + \frac{1-\eta_1}{m} \le y_1 \le 1
\end{aligned}
\right\} \quad (26)
$$

$$
\left.
\begin{aligned}
m_y^*(y_1, \eta_1) &= q\frac{c_R^2}{\beta}\left(-\frac{\lambda m}{3\pi}\left\{\frac{m^2(1-y_1)^3}{(m^2-1)^{3/2}}\tan^{-1}R_2 + \right.\right. \\
&\quad \frac{1}{m^2-1}\left[m^2(1-\eta_1)(y_1-\eta_1) - \frac{(1-\eta_1)^2}{2} - \frac{m^2(y_1-\eta_1)^2}{2}\right]R_3 - \\
&\quad \left.\left. m^2(y_1-\eta_1)^3\tanh^{-1}K_2\right\} - \frac{\beta}{2qc_R^3}u_\theta^*(y_1, \eta_1)\right), \\
&\qquad \eta_1 - \frac{1-\eta_1}{m} \le y_1 < \eta_1 + \frac{1-\eta_1}{m} \\
m_y^*(y_1, \eta_1) &= q\frac{c_R^2}{\beta}\left(-\frac{2m(m^2-1)}{3(m^2-1)^{3/2}}(1-y_1)^3\right), \\
&\qquad \eta_1 + \frac{1-\eta_1}{m} \le y_1 \le 1
\end{aligned}
\right\} \quad (27)
$$

$$
\begin{aligned}
n_y^*(y_1, \eta_1) = q\,\frac{\sigma_R^2}{\beta}\Bigg(-\frac{8m}{\pi}\Bigg\{&\frac{m^2}{(m^2-1)^{3/2}}\,\frac{(1-y_1)^4}{12}\tan^{-1}R_2 - \\
&\frac{1}{24(m^2-1)}\Big[(1-m^2)(1-\eta_1)^3 + 2(1-m^2)(y_1-\eta_1)^3 + \\
&m^2(1-y_1)^3\Big]R_3 + \Big[\frac{y_1-\eta_1}{12} - \frac{1-\eta_1}{3}\Big]m^2(y_1-\eta_1)^3\tanh^{-1}R_2 + \\
&\frac{1}{6}\,\frac{(1-y_1)^4}{\sqrt{m^2-1}}\tan^{-1}R_2 - \frac{2}{3}(y_1-\eta_1)\Big[\frac{13}{24}(1-\eta_1)^2 - \\
&\frac{7}{16}(1-\eta_1)(y_1-\eta_1) + \frac{1+2m^2}{24}(y_1-\eta_1)^2\Big]R_3 + \\
&\frac{2}{3}(y_1-\eta_1)\Big[(1-\eta_1)^2\Big(1-\frac{3}{2}y_1+\frac{\eta_1}{2}\Big) + \\
&\frac{(y_1-\eta_1)^2(m^2+2)}{2}\Big(1-\frac{3}{4}\eta_1-\frac{y_1}{4}\Big)\Big]\tanh^{-1}R_2\Bigg\}\Bigg), \\
&\qquad \eta_1 - \frac{1-\eta_1}{m} \le y_1 \le \eta_1 + \frac{1-\eta_1}{m}
\end{aligned}
\tag{28}
$$

$$
n_y^*(y_1, \eta_1) = q\,\frac{\sigma_R^2}{\beta}\left(-\frac{m(3m^2-2)}{3(m^2-1)^{3/2}}(1-y_1)^4\right),
$$

$$
\eta_1 + \frac{1-\eta_1}{m} \le y_1 \le 1
$$

where

$$R_2 \equiv \sqrt{\frac{(m-1)\left[1 + my_1 - \eta_1(1+m)\right]}{(m+1)\left[1 - my_1 - \eta_1(1-m)\right]}} \tag{29}$$

$$R_3 \equiv \sqrt{(1-\eta_1)^2 - m^2(y_1 - \eta_1)^2} \tag{30}$$

$$\left.\begin{aligned} K_2 &\equiv \sqrt{\frac{1 + my_1 - \eta_1(1+m)}{1 - my_1 - \eta_1(1-m)}}, \qquad \eta_1 - \frac{1-\eta_1}{m} \le y_1 \le \eta_1 \\ &\equiv \sqrt{\frac{1 - my_1 - \eta_1(1-m)}{1 + my_1 - \eta_1(1+m)}}, \qquad \eta_1 \le y_1 < \eta_1 + \frac{1-\eta_1}{m} \end{aligned}\right\} \tag{31}$$

In the preceding sets of indicial load equations, both subsonic and supersonic leading edges, it is seen that the quantities enclosed by the large parentheses $\left(\quad\right)$ are nondimensional and depend only upon the modified aspect-ratio parameter m. These nondimensional functions have the character of aerodynamic influence coefficients, and it is feasible to calculate and tabulate them for various values of m at discrete spanwise stations.

V. DISCUSSION

Although the selection of the angle-of-attack distribution (equation (1)) was guided by a structural deformation analysis, it is seen that the generality of the angle-of-attack distribution is not restricted to structural considerations. That is, by proper choice of $\theta(y_1)$ and $\gamma(y_1)$ the loading resulting from many angle-of-attack distributions is immediately obtained, if the loading resulting from the angle of attack of the fuselage can be neglected. This restriction is necessary because the fuselage section was assumed to be held at zero angle of attack in the analysis. For example, the lift on the delta wing at constant symmetrical angle of attack is given by:

$$\alpha\left[l_\theta^*(y_1, 0) + l_\theta^*(-2a - y_1, 0)\right]$$

However, the solution of such specific problems is readily obtained by simpler methods. In an aeroelastic analysis similar to that in reference 3, the local twist shape involving $\theta(y_1)$ and $\gamma(y_1)$ is one of the unknowns to be determined and hence the arbitrary form must be retained.

One of the common steady-state aeroelastic phenomenon is the loss of aileron effectiveness in connection with the rolling behavior of a wing. The antisymmetrical superposition of the loading functions given here is immediately applicable to the investigation of the rolling behavior of the delta wing, in an analysis similar to that of reference 3. In the rolling problem it is seen that the flat plate

fuselage section can be thought of as an idealization of a cylindrical fuselage is wing-body interference is neglected, thus furnishing a more practical model.

Another important steady-state aeroelastic problem is that of wing torsional divergence. It is believed that the symmetrical superposition of the indicial loading functions will furnish the basis for an investigation of divergence of the delta wing.

VI. SUMMARY

The aerodynamic loading of a delta wing having a linearly varying chordwise angle-of-attack distribution given by

$$\alpha(x_1, y_1) = \theta(y_1) + x_1 c_R \gamma(y_1)$$

where $\theta(y_1)$ and $\gamma(y_1)$ are arbitrary spanwise functions has been obtained. It is given in influence function form for indicial angle-of-attack distributions and the arbitrary spanwise variation of the angle of attack is accounted for by superposition in the form of a Duhamel's integral. Possible applications of the results in aeroelastic analysis have been presented and discussed.

VII. ACKNOWLEDGMENTS

The author wishes to express his appreciation to the National Advisory Committee for Aeronautics for the opportunity to use material in this thesis which was obtained from a research project conducted at their Langley Laboratory.

In particular, the author wishes to express his gratitude to Mr. John M. Hedgepeth and Mr. William W. Davenport of the Structures Research Division for their advice and assistance in performing the analysis incorporated in this thesis.

He also wishes to thank Dr. Y. K. Pian of the Applied Mechanics Department of the Virginia Polytechnic Institute for his advice and assistance in preparing this thesis.

VIII. BIBLIOGRAPHY

1. Stein, Manuel E., Hedgepeth, John M., and Anderson, J. Edward: Deflection and Stress Analysis of Thin, Solid Delta Wings of Arbitrary Planform With Particular Reference to Delta Wings. NACA Report 1131, 1953.

2. Frick, C. W., and Chubb, R. S.: The Longitudinal Stability of Elastic Swept Wings at Supersonic Speed. NACA Report 965, 1950.

3. Hedgepeth, John M., and Kell, Robert J.: Rolling Effectiveness and Aileron Reversal of Rectangular Wings at Supersonic Speeds. NACA TN 3067, 1954.

4. Evvard, John C.: Use of Source Distributions for Evaluating Theoretical Aerodynamics of Thin, Finite Wings at Supersonic Speeds. NACA Report 951, 1950.

5. Bisplinghoff, R. L., Ashley, Holt, and Halfman, R. L.: Aeroelasticity. Addison-Wesley Publishing Company, Inc., 1955.

IX. VITA

The author was born in Welch, West Virginia on December 21, 1933. He moved to Virginia in 1942 and graduated from Thomas Jefferson High School in Richmond, Virginia in 1950. The following September he entered the Virginia Polytechnic Institute and received the Degree of Bachelor of Science in Mathematics from that institution in June 1954. After graduation, he was employed by the Structures Research Division of the National Advisory Committee for Aeronautics. In the summer of 1955, he returned to the Virginia Polytechnic Institute to begin studies toward the Degree of Master of Science in Applied Mechanics.

XI. APPENDICES

APPENDIX A. Determination of Potential of a Thin, Finite Wing at a Given Angle of Attack

In reference 4, in connection with the determination of the lift of a thin wing at supersonic speeds, Evvard evolved a general lifting surface theory which is applicable to thin wings of arbitrary plan form and cross section in steady or unsteady flow. For the purposes of expediting the present thesis, the elements of his work presented here will be limited in scope so that they apply only to a triangular wing of symmetrical cross section in steady flow.

Evvard considered the wing as a thin surface sustaining pressure differences and replaced the flow field between the leading edge of the wing and the foremost Mach wave (if such a field exists), with an imaginary diaphragm which cannot sustain pressure differences. Over all, a sheet of supersonic sources is spread with strengths proportional to the local slope of the surface of diaphragm.

By a limiting process, it is then shown that the potential at a point on the upper or lower surface is obtained by integrating this source potential distribution over the areas of wing surface and diaphragm contained within the Mach forecone of the point. This scheme is used to evaluate the potential at a point on the upper and lower surfaces of the flow field diaphragm. Application of the Bernoulli equation specifying no pressure difference in this area yields a relationship between the local slopes of the wing surface and those of

the diaphragm contained within the Mach forecone of the point under consideration. This relationship is used in evaluating the potential of a point on a thin wing of symmetrical cross section influenced by a single isolated external flow field. It is then shown that the integration over the portion of the flow field contained within the Mach forecone of the point exactly cancels that over the portion of the wing which generated the flow field.

This is illustrated in Figure 5. There, it is desired to calculate the potential at a point in the vicinity of a wing tip of symmetrical cross section with a subsonic leading edge. For a point (x_1, y_1) in this region, the potential would normally be calculated by integrating over the entire area within the Mach forecone of the point, that is, over S_{W_1}, S_{W_2}, and S_{D_1}, as shown. However, the analysis of Evvard shows that the integration over S_{D_1} exactly cancels that over S_{W_1}, or that the potential is determined by integrating over S_{W_2} only. This indicates that the wing area S_{W_1} gives rise to the flow field area S_{D_1} since the potential is identical to that which would be obtained if the wing were cut off along line AB. It is seen that the inboard boundary of points (x_1, y_1) thus affected can be established by reflecting the Mach wave. For points (x_2, y_2) to the left of this boundary, the potential is obtained by integrating over S_{W_3} the entire wing area within the Mach forecone of the point.

For the triangular plan-form wings considered in this report, the presence (or absence) of an external flow field of the type described is found to depend on the character of the Mach number of

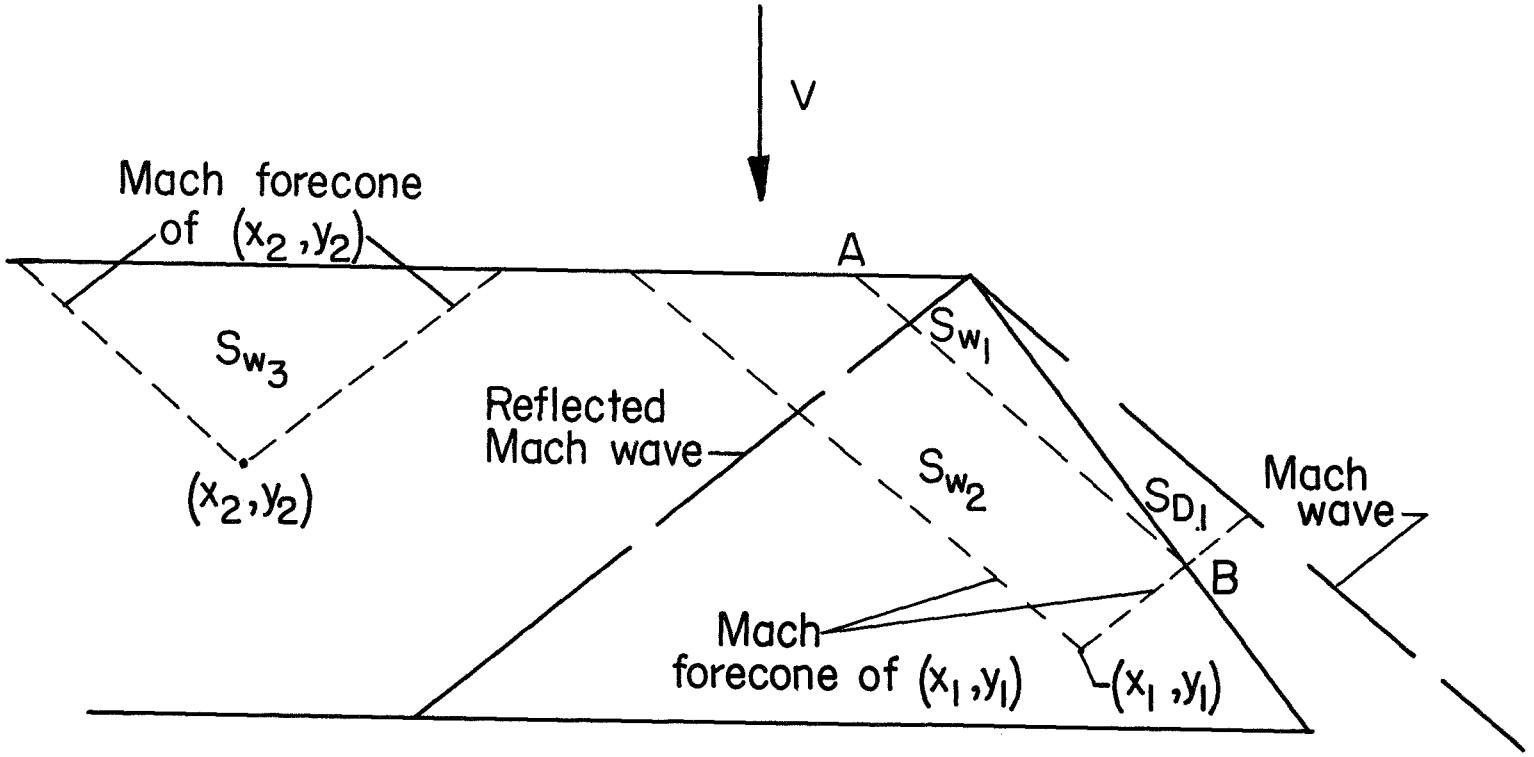

Figure 5.- Illustration of Evvard's theories for thin wings of symmetrical cross section influenced by a single external flow field.

the normal flow velocity of the leading edge. If the velocity component is subsonic, the leading edge is said to be subsonic and the foremost Mach wave lies ahead of the leading edge. Hence there does exist an external flow field between the leading edge of the wing and the foremost Mach wave. However, if the normal velocity is supersonic, the envelope of the foremost Mach waves is coincident with the leading edge. In this case there is no external flow field, and the potential at a point on the wing is obtained by simply integrating over the portion of the wing contained within the Mach forecone of the point.

At this point it is convenient to introduce the modified aspect-ratio parameter $m = \frac{\beta l}{c_R}$. For $m < 1$ the leading edge is seen to be subsonic, while for $m > 1$ it is supersonic. Moreover it is seen from Figure 5 that, as long as the end of the reflected Mach wave passes through the trailing edge of the delta configuration, points on the wing surface are influenced by at most a single flow field. The lower boundary of m for which this is true, that is, $m = \frac{1}{1 + 2a}$ is seen to correspond to the value of m at which the reflected Mach wave passes through the tip of the opposite wing. Although Evvard's theories can be extended to apply to the delta wing for $m < \frac{1}{1 + 2a}$, the range of applicability of the results is reduced considerably, and these cases will not be considered here.

In each case the common symbol S_R will be used to designate the area of integration. Therefore the potential at a point on the wing

resulting from an angle-of-attack distribution of $\sigma(x_1, y_1)$ is given in nondimensional coordinates by Evvard as

$$\phi_\sigma(x_1, y_1) = \frac{V_1}{\pi} \iint_{S_E} \frac{\sigma(\xi_1, \eta_1) d\xi_1 \, d\eta_1}{\sqrt{(x_1 - \xi_1)^2 - m^2(y_1 - \eta_1)^2}} \tag{A1}$$

APPENDIX B. Determination of Lift of a Thin, Finite Wing at an Arbitrary Angle of Attack

It is desired to determine the lift resulting from an arbitrary spanwise angle-of-attack distribution over a wing. One solution to this problem would be the direct superposition of the lift resulting from impulsive angles of attack. However, an impulsive angle of attack of this kind gives rise to infinite pressures and the resulting difficulties of analysis. A more promising approach is that of a Duhamel's integral fundamental to linear systems and usually associated with linear time dependent phenomena. Basically it is a process of step-superposition and was first used in connection with the determination of lift due to an arbitrary angle-of-attack distribution by Frick and Chubb (reference 2). It was later successfully incorporated in an aeroelastic analysis of a rectangular wing by Hedgepeth and Kell (reference 3).

No mathematical analysis was given in the former reports, however, and it is believed that such an analysis is needed in order to fully understand the method. It is therefore given here with reference to the lift imposed by an arbitrary angle of attack of $\theta(y_1)$ with the restriction that $\theta(0) = 0$ that is, no root deformation. A typical variation of $\theta(y)$ with span is shown in Figure 6. The span is divided into N increments of lengths $\Delta\eta_i$ $(i = 0, 1, 2 \ldots N)$ by the abscissi, η_i, such that $\eta_N = 1$. The increments are defined by

$$\Delta\eta_i = \eta_{i+1} - \eta_i \qquad (i = 0,1,2 \ldots N) \tag{B1}$$

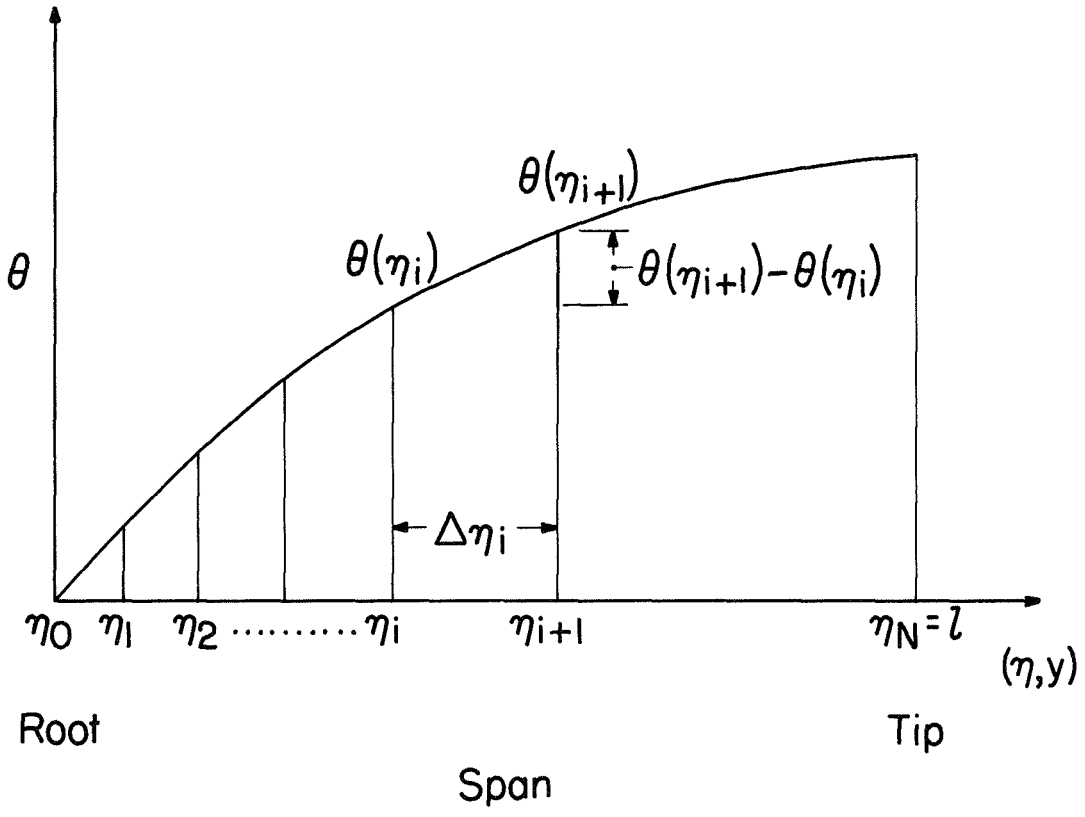

Figure 6.- Typical variation of θ with span.

If the lift distribution resulting from a unit step angle of attack of $1(y - \eta)$ defined as $l_\theta^*(y, \eta)$, then the lift resulting from a step angle of attack of magnitude $\theta(\eta_{i+1}) - \theta(\eta_i)$ applied at the spanwise station η_{i+1} is given by

$$\left[\theta(\eta_{i+1}) - \theta(\eta_i)\right] l_\theta^*(y, \eta_{i+1}) = \frac{\theta(\eta_i + \Delta\eta_i) - \theta(\eta_i)}{\Delta\eta_i} l_\theta^*(y, \eta_i + \Delta\eta_i)\Delta\eta_i \tag{B2}$$

and the lift furnished by the aggregate of steps is then

$$\sum_{i=0}^{N-1} \frac{\left[\theta(\eta_i + \Delta\eta_i) - \theta(\eta_i)\right]}{\Delta\eta_i} l_\theta^*(y, \eta_i + \Delta\eta_i)\Delta\eta_i \tag{B3}$$

In the limit as $N \longrightarrow \infty$ and $\Delta\eta_i \longrightarrow 0$ simultaneously, the lift resulting from the given angle-of-attack distribution of $\theta(y)$ is given by

$$l_\theta^*(y) = \lim_{\substack{N \to \infty \\ \Delta\eta_i \to 0}} \sum_{i=0}^{N-1} \frac{\left[\theta(\eta_i + \Delta\eta_i) - \theta(\eta_i)\right]}{\Delta\eta_i} l_\theta^*(y, \eta_i + \Delta\eta_i)\Delta\eta_i \tag{B4}$$

and by the definition of $\frac{d\theta}{d\eta}$ and the Riemann integral, it follows that

$$l_\theta^*(y) = \int_0^l l_\theta^*(y, \eta) \frac{d\theta(\eta)}{d\eta} d\eta \tag{B5}$$

or in nondimensional coordinates $y_1 = \frac{y}{l}$, $\eta_1 = \frac{\eta}{l}$

$$i_\theta^*(\gamma_1) = \int_0^1 i_\theta^*(\gamma_1, \eta_1) \frac{d\theta(\eta_1)}{d\eta_1} d\eta_1 \qquad (36)$$